Chemistry Europe
European Chemical Societies Publishing

WILEY VCH

Excellence in Chemistry Research

Announcing our new flagship journal

- Gold Open Access
- Publishing charges waived
- Preprints welcome
- Edited by active scientists

Meet the Editors of *ChemistryEurope*

Luisa De Cola
Università degli Studi di Milano Statale, Italy

Ive Hermans
University of Wisconsin-Madison, USA

Ken Tanaka
Tokyo Institute of Technology, Japan

Check for updates

ChemistrySelect

Research Article
doi.org/10.1002/slct.202301786

Chemistry Europe
European Chemical Societies Publishing

www.chemistryselect.org

New Coumarin–Thiosemicarbazone Based Zn(II), Ni(II) and Co(II) Metal Complexes: Investigation of Cholinesterase, α-Amylase, and α-Glucosidase Enzyme Activities, and Molecular Docking Studies

Esra Çelik,[a] Mücahit Özdemir,[a] Baybars Köksoy,[b] Tugba Taskin-Tok,[c, d] Parham Taslimi,*[e] Nastaran Sadeghian,[e] and Bahattin Yalçın*[a]

New coumarin–thiosemicarbazone compounds and their zinc(II), nickel(II), and copper(II) metal complexes were synthesized and characterized. The inhibitory activities of these new coumarin–thiosemicarbazone-based metal complexes against butyrylcholinesterase (BChE), acetylcholinesterase (AChE), α-amylase, and α-glucosidase were determined. The results showed that all the synthetic compounds exhibited potent inhibitory activities against all targets, as compared to the standard inhibitors, as revealed by the half-maximal inhibitory concentration (IC_{50}) and the inhibitory constant (*Ki*) values. The *Ki* values of the new complexes for BChE, AChE, and α-glucosidase enzymes were obtained in the ranges of 115.84–276.07, 31.68–117.08, and 22.56–47.82 μM, respectively. Moreover, molecular docking studies provided support for the conclusion that coumarin–thiosemicarbazone zinc(II) (−102.34; −10.41 kcal/mol) and coumarin–thiosemicarbazone cobalt(II) complexes (−25.46; −9.49 kcal/mol) act as dual inhibitors for both AChE and α-amylase species. Furthermore, coumarin–thiosemicarbazone cobalt(II) (−39.46 kcal/mol) and coumarin–thiosemicarbazone nickel(II) complexes (−39.41 kcal/mol) demonstrated potential as inhibitors of α-glucosidase. Of all the compounds studied, bis-3-benzyl-7,8-dimethoxycoumarin–thiosemicarbazonato zinc(II) is the most potent drug against AChE.

Introduction

Coumarins are an important class of organic compounds that include a lactone ring isolated from the Tonka bean.[1] Coumarins have many advantages, such as high fluorescent quantum yield, large Stokes shift, excellent light stability, and less toxicity.[2] In addition, coumarins exhibit biological effects such as antibacterial,[3] anti-cancer,[4] antiviral,[5] and anticoagulant.[6]

Thiosemicarbazones are a class of compounds that contain nitrogen and sulfur donor atoms in their structure which are obtained by the reaction of thiosemicarbazide with aldehydes or ketones.[7] These donor atoms in their structure make thiosemicarbazones a suitable ligand, enabling them to coordinate well with metals and advance from the presence of amides, imines, and thiol groups with polydentate ligand features.[8,9]

The biological activities of thiosemicarbazones and their have changed according to the aldehyde and ketone groups, and the metal atom. In addition.[10] Thiosemicarbazones and transition metals have important biological activities such as antidiabetic,[11] antifungal,[12] antimicrobial,[13] anti enzymatic,[14] anticancer,[15] and antioxidants.[16]

α-Glycosidase is an enzyme that functionally hydrolyzes carbohydrate molecules to generate α-glucosidase of complex carbohydrates and to produce existing candies in the process of catabolic metabolism. This enzyme plays a delay in the absorption of glucose by increasing the release of insulin to postprandial β cells, thus playing an effective role in suppressing the rise of the postprandial blood glucose level. Type 2 diabetes is used as a method of treatment for various diseases such as cancer, HIV, hepatitis, and obesity.[17] Acetylcholinesterase (AChE) and Butyrylcholinesterase (BChE) enzymes prevent nerve impulse conduction in cholinergic synapses by providing catalytic hydrolysis of acetylcholine (ACh) and butyrylcholine (BCh) the neurotransmitters. BChE, which is synthesized in the liver and existed in muscle tissues, functions as a joint regulator

[a] *E. Çelik, M. Özdemir, Prof. Dr. B. Yalçın*
Department of Chemistry
Marmara University
34722 Kadikoy Istanbul, Türkiye
E-mail: byalcin@marmara.edu.tr

[b] *Asst. Prof. Dr. B. Köksoy*
Department of Chemistry
Bursa Technical University
16310 Yildirim, Bursa, Türkiye

[c] *Assoc. Prof. Dr. T. Taskin-Tok*
Department of Chemistry
Gaziantep University
27310 Sehitkamil, Gaziantep, Türkiye

[d] *Assoc. Prof. Dr. T. Taskin-Tok*
Department of Bioinformatics and Computational Biology
Gaziantep University
27310 Sehitkamil, Gaziantep, Türkiye

[e] *Assoc. Prof. Dr. P. Taslimi, Asst. Prof. Dr. N. Sadeghian*
Department of Biotechnology
Bartin University
74100 Merkez, Bartin, Türkiye
E-mail: ptaslimi@bartin.edu.tr

Supporting information for this article is available on the WWW under https://doi.org/10.1002/slct.202301786

© 2023 Wiley-VCH GmbH

of AChE as an enzyme that helps the AChE enzyme.[18] Anticholinesterase drugs by reversible or irreversibly inhibiting the AChE, are a path referenced in the treatment of diseases such as Senile Dementia, Parkinson, Alzheimer, and Myasthenia Gravis.[19]

Karcz *et al.*, synthesized coumarin–thiadiazole hybrids and their Cu(II) and Zn(II) metal complexes and tested them as acetylcholinesterase inhibitors. They obtained weak but promising inhibition from these compounds.[20] Onar *et al.*, investigated the enzyme activities of coumarin–chalcone derivatives against acetylcholinesterase, α-glycosidase, and carbonic anhydrase. Most chalcone–coumarin derivatives was reported to have much better inhibition values than the reference compound acetazolamide for carbonic anhydrase. For acetylcholinesterase, all derivatives have better inhibition than tacrine. For α-glycosidase, the chalcone–coumarin derivative containing phenyl groups has the best inhibition value, including acarbose.[21] Amin *et al.*, tested a variety of natural and synthetic coumarins, including thiosemicarbazone derivatives, as acetylcholinesterase (AChE) inhibitors. They used donepezil as a reference compound and discussed the structure-activity relationships of the coumarins. In general, the compounds showed better inhibition than donepezil at the micromolar level, with the thiosemicarbazone–coumarin compound having the best value.[22] Hamulakova *et al.*, investigated the cholinesterase (AChE and BChE) activities of Tacrine–coumarin hybrids. The Tacrine–coumarin hybrids showed inhibitory activity against both AChE and BChE with IC_{50} values ranging from micromolar to submicromolar concentrations. Based on the results, the Tacrine–coumarin hybrids were reported to have a stronger acetylcholinesterase activity than butyrylcholinesterase activity.[23] For AChE, the coumarins exhibited moderate inhibitory activity compared to Galanthamine, but no inhibition was observed for α-glucosidase.[24] Based on this literature summary, structural activity relationships can be established to identify potential inhibitors for these enzymes.

In addition, this study aims to combine two important compound classes, such as coumarin and thiosemicarbazone, in a single hybrid structure based on the structure-activity relationships of coumarins on relevant enzymes in the literature, and to discover potential drugs by increasing the AChE, BChE, α-glucosidase, and α-amylase enzyme activities of this hybrid structure and its metal complexes. The enzyme activity values will be a guide and support for scientists working in this field to discover drugs.

Results and Discussion

Characterization

In this study, 7,8-dihydroxy-3-benzoylcoumarin and 4-phenyl thiosemicarbazide compounds were synthesized according to the literature,[25] and the new (E)-2-((7,8-dimethoxy-2-oxo-2*H*-chromen-3-yl)(phenyl)methylene)-*N*-phenylhydrazine-1-carbothioamide was obtained by the reaction of these two compounds. Then, zinc, nickel, and cobalt metal complexes of (E)-2-((7,8-dimethoxy-2-oxo-2*H*-chromen-3-yl)(phenyl)methylene)-*N*-phenylhydrazine-1-carbothioamide were synthesized. The structure of the coumarin–thiosemicarbazone ligand was characterized by spectroscopic methods such as FT-IR, UV-Vis, ^{1}H-NMR, ^{13}C-NMR spectroscopies, single crystal X-Ray diffraction, and MALDI-TOF mass spectrometry. The structure of coumarin–thiosemicarbazone metal complexes, FT-IR, UV-Vis, and MALDI-TOF mass spectrometry was evaluated.

In the FT-IR spectrum of the (E)-2-((7,8-dimethoxy-2-oxo-2*H*-chromen-3-yl)(phenyl)methylene)-*N*-phenylhydrazine-1-carbothioamide (**2**), the carbonyl group stretching (C=O) in the structure showed a sharp vibration band at 1717 cm^{-1}. The vibration bands at 1604 cm^{-1}, 1366 cm^{-1}, and 3290 cm^{-1} are specific bands belonging to the υ(C=N), υ(C=S), and υ(N–H) functional groups, respectively. The carbonyl band (C=O) was observed as a shoulder and shifted from 1717 to 1643 cm^{-1} in the zinc, cobalt, and nickel metal complexes. This decrease in the carbonyl band suggests that the carbonyl groups are involved in chelation.[26] The bands belonging to the υ(C=N) shifted to 1590 cm^{-1} (shifted 14 cm^{-1}) for **2a**, 1586 cm^{-1} (shifted 18 cm^{-1}) for **2b** and 1591 cm^{-1} (shifted 13 cm^{-1}) for **2c**. The bands belonging to the υ(C=S) shifted to 1285 cm^{-1} (shifted 81 cm^{-1}) for **2a**, 1290 cm^{-1} (shifted 76 cm^{-1}) for **2b** and 1289 cm^{-1} (shifted 77 cm^{-1}) for **2c**. This means that the N and S atoms were coordinated with the metals. In addition, the disappearance of the υ(N–H) peak in the IR spectra of metal complexes also supports the formation of complexes. In addition to these, the υ(M–O) band was observed around 400 cm^{-1} and the υ(M–N) band around 500 cm^{-1} for metal complexes.

^{1}H-NMR and ^{13}C-NMR spectra of compounds were taken using DMSO-d_6. In the ^{1}H-NMR spectrum of the 3-benzoyl-7,8-dimethoxy-coumarin (**1**), the peaks of the two methoxy groups in the benzene ring of the coumarin were observed as a singlet at 3.98 and 3.90 ppm, and the other peaks of the ring were doublet at 7.22 and 7.63–7.61 ppm. The proton peak at the C-4 position of coumarin was observed as a singlet at 8.37 ppm. Peaks to the benzene ring in the structure were observed as a multiplet at 7.58–7.53, 7.71–7.66 ppm, and a doublet at 7.92 ppm. The ^{13}C-NMR spectrum of the coumarin matched the 18 carbons with the structure. In the ^{1}H-NMR spectrum of the **2**, the peaks of the protons in the benzene ring attached to the terminal nitrogen atom were observed as a multiplet at 7.45–7.38 ppm. Two protons belonging to the secondary amine group in the structure were observed as a singlet at 10.26 and 11.29 ppm. In the ^{13}C-NMR spectrum, peaks belonging to the methoxy group are observed at 57.04 and 61.34 ppm. The peak of the (C=S) group is at 177.63 ppm. The carbonyl (C=O) peak of the coumarin is at 158.70 ppm. Aromatic carbon peaks of the coumarin–thiosemicarbazone compound are between 156.29 and 109.21 ppm.

The molecular ion peaks of **2** and **2c** were observed as 460.73 *m/z* and 975.39 *m/z*, respectively, in MALDI-TOF-MS taken using 2,5-dihydroxybenzoic acid (DHB) matrix. Again, in other mass spectra taken with the dithranol (DIT) matrix, the molecular ion peaks of the compounds are 976.92 *m/z* for **2a** and 975.39 *m/z*, 982.30 *m/z* for **2b**, respectively. These values in

© 2023 Wiley-VCH GmbH

23656549, 2023, 38, Downloaded from https://chemistry-europe.onlinelibrary.wiley.com/doi/10.1002/slct.202301786 by Marmara University, Wiley Online Library on [06/11/2023]. See the Terms and Conditions (https://onlinelibrary.wiley.com/terms-and-conditions) on Wiley Online Library for rules of use; OA articles are governed by the applicable Creative Commons License

the mass spectra suit the molecular weights of the proposed structures.

UV-Vis spectra of compounds (**2a**–**2c**) were studied in the range of 250–800 nm using DMSO. The main band at 350 nm and the second band at 260 nm were observed in the UV-Vis spectrum of 3-benzoyl-7,8-dimethoxy-coumarin. The long wavelength absorption band is associated with $\pi\rightarrow\pi^*$ and $n\rightarrow\pi^*$ electronic transitions involving the electron pair of the exocyclic oxygen atom (C=O). The observed absorption bands are the characteristic $\pi\rightarrow\pi^*$ electronic transition for coumarin compounds.[27] When thiosemicarbazone is substituted to the structure, the main band shifted to 328. The absorption spectrum of compound **2** is blue-shifted due to the electron-withdrawing abilities of the nitrogen and sulfur atoms on the thiosemicarbazone.[28] When the coumarin–thiosemicarbazone ligand was complexed with zinc, nickel, and cobalt metals, it showed a single band with a peak of 277 nm.[26c] On the other hand, it is understood from the UV-Vis spectrum that the charge transfer band (LMCT), which shows that the sulfur and nitrogen atoms in the ligand are coordinated to the metal, is observed at around 485 nm, with a less intensity in zinc and a more pronounced red shift in cobalt and nickel (Figure 1).

X-ray structural determination

Single-crystal X-ray structural analysis method was used to obtain detailed predictions about starting coumarin (**1**) and coumarin–thiosemicarbazide (**2**) solid-state structures, molecular conformation, packing, and intermolecular interactions. The compound **1** was crystallized in an ethyl acetate/hexane mixture, and compound **2** was crystallized in acetone at room conditions. Compound **1** crystallizes in triclinic *P*-1 and compound **2** in monoclinic space group $P2_1/c$ (Table 1). The ORTEP diagram along with the atom-labelling scheme for compounds **1** and **2** is given in Figure 2.

Bond distances (Å), angles (°), and dihedral angles (°) for **1** and **2** were supplied in Tables S2–S11. While no hydrogen bond interaction was observed for the coumarin compound (**1**), it was observed for the (**2**) compound (O4···N2 = 2.719 Å). For **1**, two C–H···O (2.556 and 2.718 Å) and one C–H···C (2.898 Å) short contacts were observed between the two coumarin skeletons (Figure 3). For **2**, two C···S (3.484 and 3.414 Å) and one N–H···S (2.814 Å) short contacts were observed between the two coumarin–thiosemicarbazide (Figure 4). The 3-benzoyl-7,8-dimethoxy-coumarin crystal is packaged in herringbone (Figure 3). In crystal **1**, the acetophenone group attached to the coumarin at the C-3 position is located at an angle of 59.51° to the coumarin skeleton. In crystal **2**, when it is substituted with thiosemicarbazide, it is positioned at 56.49°. Other bond distances (Å) and angles (°) parameters of coumarins have similar values to coumarin and its derivatives in the literature.[29]

Enzyme Activities

α-Glucosidase inhibitors work by competitive and reversible inhibition of these intestinal enzymes. It slows down the

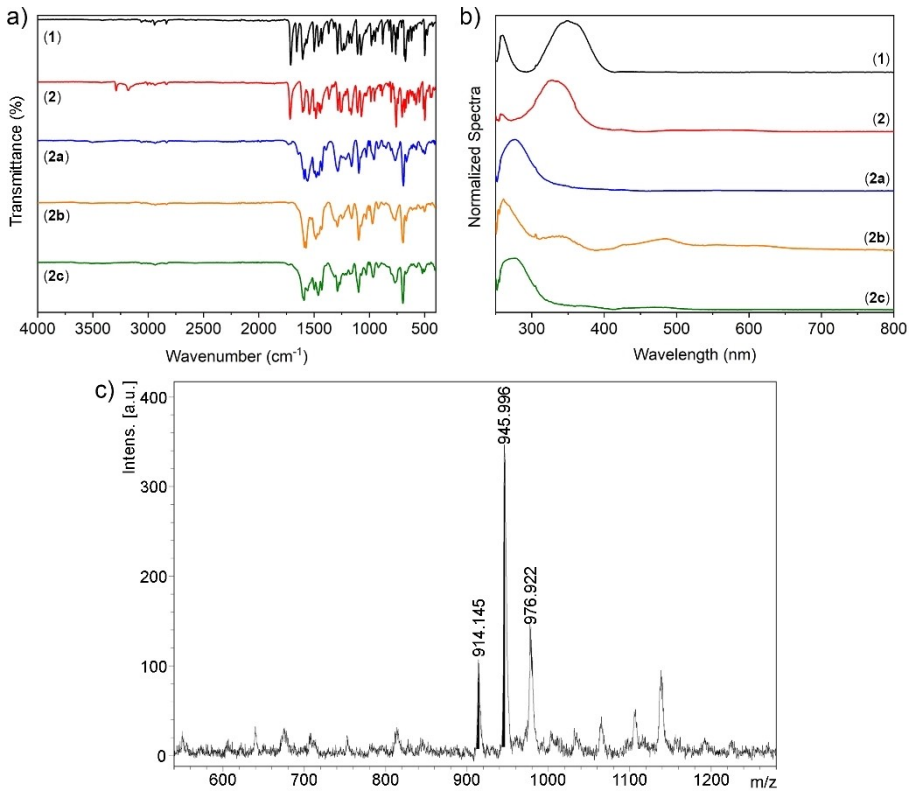

Figure 1. The FT-IR (a) and UV-Vis (b) spectra of synthesized compounds (**1**,**2** and **2a**–**c**). (c) The MALDI-TOF-mass spectrum of complex **2c** using DIT matrix.

© 2023 Wiley-VCH GmbH

23656549, 2023, 38, Downloaded from https://chemistry-europe.onlinelibrary.wiley.com/doi/10.1002/slct.202301786 by Marmara University, Wiley Online Library on [06/11/2023]. See the Terms and Conditions (https://onlinelibrary.wiley.com/terms-and-conditions) on Wiley Online Library for rules of use; OA articles are governed by the applicable Creative Commons License

23656549, 2023, 38, Downloaded from https://chemistry-europe.onlinelibrary.wiley.com/doi/10.1002/slct.202301786 by Marmara University, Wiley Online Library on [06/11/2023]. See the Terms and Conditions (https://onlinelibrary.wiley.com/terms-and-conditions) on Wiley Online Library for rules of use; OA articles are governed by the applicable Creative Commons License

Table 1. Crystal and structure refinement data of compounds **1** and **2**.

	1	**2**
CCDC	2214759	2214757
Chemical formula	$C_{25}H_{21}N_3O_4S$	$C_{18}H_{14}O_5$
Formula weight	459.51	310.29
Temperature/K	273.15	296.15
Crystal system	triclinic	monoclinic
Space group	*P*-1	*P*21/c
a/Å	10.4105(13)	4.1265(6)
b/Å	10.7882(13)	15.623(2)
c/Å	10.9071(14)	22.860(3)
α/°	76.187(2)	90
β/°	65.534(2)	90.513(3)
γ (°)	82.129(2)	90
Volume/Å^3	1081.7(2)	1473.7(4)
Z	2	4
ρ_{calc}g/cm^3	1.411	1.399
μ/mm^{-1}	0.189	0.103
F(000)	480.0	648.0
Crystal size/mm^3	0.205×0.116 × 0.082	0.311×0.089×0.059
Radiation	MoKα (λ = 0.71073)	MoKα (λ = 0.71073)
θ range (°)	3.892 to 49.998	3.158 to 50
Index ranges	$-12 \le h \le 12$, $-12 \le k \le 12$, $-12 \le l \le 12$	$-4 \le h \le 4$, $-18 \le k \le 18$, $-27 \le l \le 27$
Reflections collected	12324	18384
Independent reflections	3797 [R_{int} = 0.0380, R_{sigma} = 0.0352]	2577 [R_{int} = 0.1273, R_{sigma} = 0.0996]
Data/restraints/parameters	3797/0/300	2577/0/210
Goodness-of-fit on F^2	1.067	0.909
Final R indexes [$I >= 2\sigma$ (I)]	R_1 = 0.0377, wR_2 = 0.0921	R_1 = 0.0557, wR_2 = 0.1157
Final R indexes [all data]	R_1 = 0.0525, wR_2 = 0.0981	R_1 = 0.1676, wR_2 = 0.1402
Largest diff. peak/hole/e Å^{-3}	0.19/−0.23	0.17/−0.18

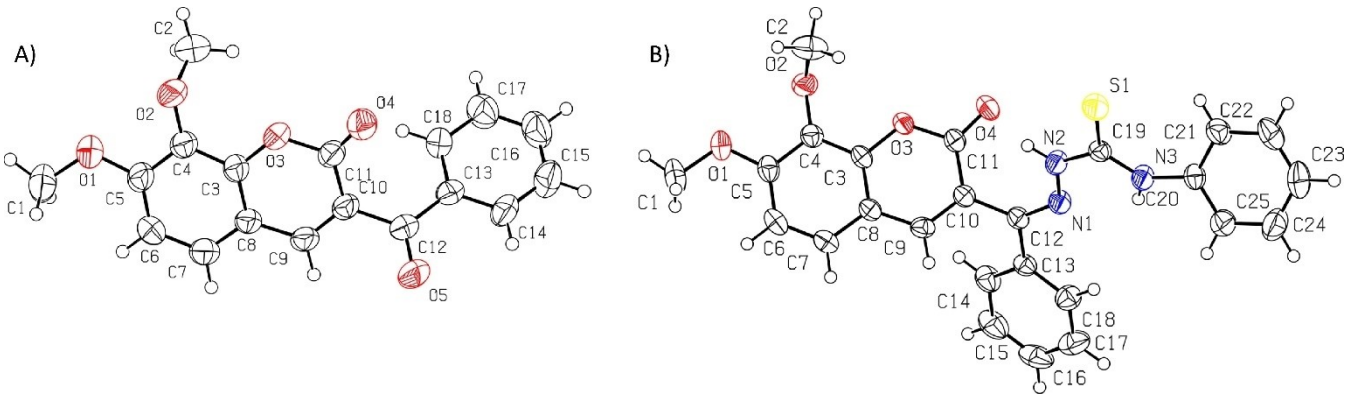

Figure 2. A view of the structure of 3-benzoyl-7,8-dimethoxy-coumarin (A) and 3-benzoyl-7,8-methoxycoumarin thiosemicarbazone (B) showing the atom-labelling scheme. Displacement ellipsoids are drawn at the 50% probability level.

digestion of carbohydrates and delays glucose absorption. This results in a smaller and slower rise in blood sugar levels, effectively after meals and throughout the day. In this study, newly synthesized compounds acted on two metabolic enzymes, and their inhibitions were determined. In the following stages of the study, *K*i values for α-glycosidase enzyme were obtained between 22.56–47.82 micromolar. In this study, the enzyme inhibition capacities of these compounds were investigated and their inhibition effects on α-amylase enzyme were investigated. The results were compared with

© 2023 Wiley-VCH GmbH

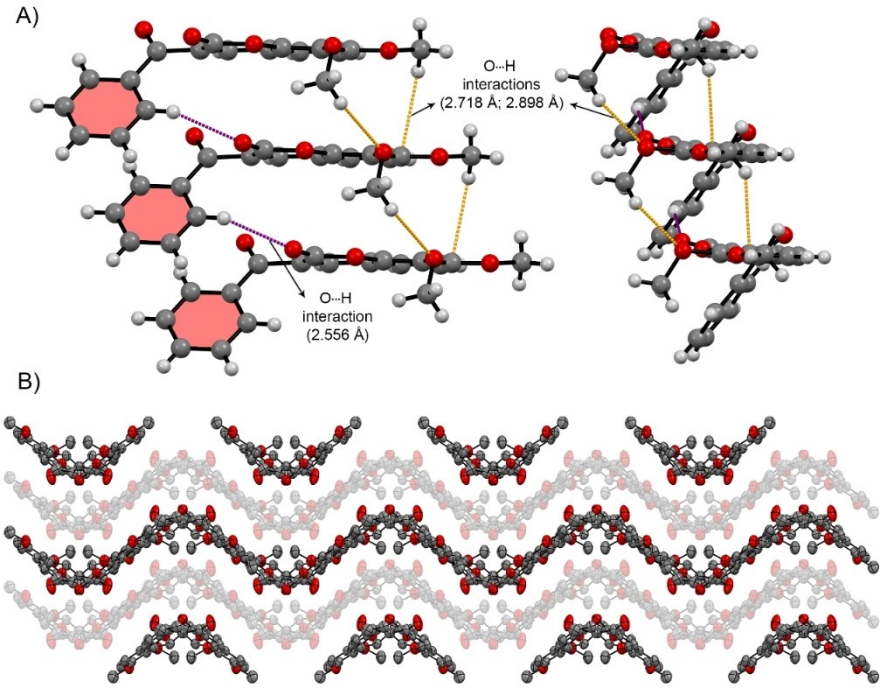

Figure 3. The crystal packing of 3-benzoyl-7,8-dimethoxy-coumarin (**1**) and intermolecular interactions.

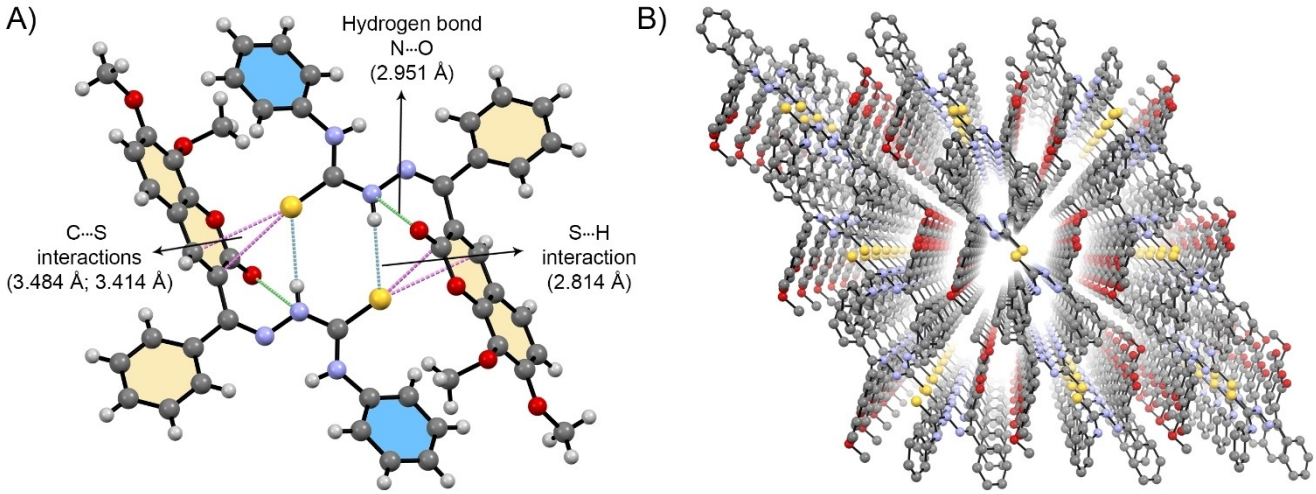

Figure 4. The crystal packing of 3-benzoyl-7,8-methoxycoumarin thiosemicarbazone (**2**) and intermolecular interactions.

standard molecules used in the respective activities. The results obtained will certainly shed light on future biochemical, physiological, and pharmacological studies in the relevant fields, and the results will have important effects on the research and treatment of many metabolic diseases such as diabetes. In this context, it is thought that some of these compounds, such as **2a**, **2b**, and **2c**, will make important contributions to the design of drugs to be used for treatment in the future and related applications. In this study, IC_{50} results for α-amylase enzyme were obtained between 13.72–61.45 micromolar. Compounds **2a**, **2b**, and **2c** were obtained as the best inhibitors for α-glycosidase and α-amylase (Table 2). If these compounds are used in drug structures, they prevent the breakdown of complex carbohydrates and disaccharides into absorbable monosaccharides in the small intestine by blocking the α-glucosidase enzyme. Positive results were obtained for acetylcholinesterase and butyrylcholinesterase, e.g., **2a**, **2b**, and **2c** compounds were detected as good inhibitors for choline esterase enzymes. The IC_{50} and *Ki* results of these good inhibitors were thus obtained, respectively, for AChE; IC_{50}: 36.93, 44.34, and 39.16, *Ki*: 31.68, 42.07, 38.44. Also, the IC_{50} and *Ki* results of these good inhibitors were obtained in this way, respectively, for BChE; IC_{50}: 155.02, 119.54, and 135.72, *Ki*: 149.31, 115.84, 129.64 μM. Compound results in all enzymes were good according to the standards, only the first and second compounds had slightly weaker effects compared to the

© 2023 Wiley-VCH GmbH

23656549, 2023, 38, Downloaded from https://chemistry-europe.onlinelibrary.wiley.com/doi/10.1002/slct.202301786 by Marmara University, Wiley Online Library on [06/11/2023]. See the Terms and Conditions (https://onlinelibrary.wiley.com/terms-and-conditions) on Wiley Online Library for rules of use; OA articles are governed by the applicable Creative Commons License

Table 2. The enzyme inhibition results of new compounds (**1**–**2**, **2a**–**2c**) against AChE, BChE, α-amylase, and α-glycosidase enzymes.

Sample	IC_{50} (μM)								*Ki* (μM)		
	AChE	r^2	BChE	r^2	α-Gly	r^2	α-Amy	r^2	AChE	BChE	α-Gly
(**1**)	93.03	0.9726	282.34	0.9806	44.13	0.9882	51.07	0.9789	88.52 ± 6.96	276.07 ± 18.08	47.82 ± 4.27
(**2**)	129.32	0.9881	262.56	0.9510	41.86	0.9863	61.45	0.9593	117.08 ± 12.67	256.08 ± 27.80	45.96 ± 3.82
(**2a**)	36.93	0.9781	155.02	0.9684	33.56	0.9722	13.72	0.9880	31.68 ± 4.17	149.31 ± 16.95	37.14 ± 6.31
(**2b**)	44.34	0.9346	119.54	0.9931	24.06	0.9598	19.94	0.9749	42.07 ± 5.88	115.84 ± 13.68	26.77 ± 4.63
(**2c**)	39.16	0.9924	135.72	0.9837	21.05	0.9020	14.36	0.9775	38.44 ± 8.11	129.64 ± 10.74	22.56 ± 3.10
TAC[a]	118.15	0.9741	191.24	0.9642	–	–	–	–	97.88 ± 20.41	176.52 ± 19.35	–
ACR[b]	–	–			64.53	0.9725	78.61	0.9825	–		71.58 ± 6.24

[a] Tacrine (TAC) is as a positive control for AChE and BChE. [b] Acarbose (ACR) is as a positive control for α-glucosidase and α-amylase.

standards. All results were obtained at the micromolar level. Besides, Hameed *et al.* synthesized coumarin-based thiosemicarbazone complexes and examined their anti-urease activity. They tested coumarin–thiosemicarbazide derivatives containing donor and acceptor subgroups over thiosemicarbazide and obtained inhibition values in the range of 2.23–43.12 μM. In metal complexes, the IC_{50} value of the coumarin–thiosemicarbazone cobalt complex containing methoxy subgroup is 116.12 μM, just like in our designs, and other metal complexes could hardly be tested.[30] Studies for such components are quite limited.

Docking Results

The binding affinity, mode, and possible types of interactions discussed in this research study give a more and good insight into the research using molecular docking calculations between the synthesized compounds (**2a**–**2c**) and AChE, BChE, α-glucosidase, and α-amylase. The results obtained are presented in Table 3.

In the study for the AChE target, Table 3 shows that the docking score energy values for the complexes bis-3-benzyl-7,8-dimethoxycoumarin–thiosemicarbazonato zinc (II) **(2a)** and bis-3-benzyl-7,8-dimethoxycoumarin–thiosemicarbazonato cobalt (II) **(2c)** were −102.34 and −25.46 kcal/mol, compared with −7.37 kcal/mol for Tacrine. The best binding affinity score was assigned to compound **2a**, which showed better binding affinity than tacrine. When we investigate the reason for this at the atomic level, it is due to the orientation of the target in the active region and the formation of sulfur-X bond (Trp286, 2.972 Å) and π-lone pair bond (Tyr124, 2.984 Å) with the sulfur atom in its structure. Compound **2c** is also more active than the reference compound because it forms more hydrogen bonds (Ser293, 1.812 Å; Gly342, 2.986 Å, and 2.742 Å) and electrostatic interactions (Glu292, 3.900 Å) and hydrophobic interactions (Tyr341, 4.724 Å, and 5.159 Å; Ala343, 2.495 Å and 3.884 Å, Val294, 4.167 Å, and 4.795 Å; Val365, 3.693 Å, and 3.344 Å; Val294, 3.843 Å; Pro344, 5.070 Å; Tyr72, 4.885 Å; Trp286, 5.421 Å, 5.479 Å, and 4.764 Å; Leu289, 3.955 Å) as given at Table S1 in the supplementary file. On the other hand, **2c** exhibits less activity than compound **2a** due to the Ni metal in its structure and its exposure in the active region of the target. These are displayed in Figure 4. Additionally, the structure of 1,2,3,4-tetrahydroacridine-9-amine (Tacrine) can lead to a lower binding affinity on the same target compared to other Zn and Co complex structures due to its lower topological surface area. These results explain why compound **2a** and **2c**, even more so than Tacrine and other compounds, exhibit certain orientations and interactions in the *in vitro* analyses. Additionally, they reveal differences in the interaction mechanisms with the target enzyme.

The binding affinity scores of two potential compounds, bis-3-benzyl-7,8-dimethoxycoumarin–thiosemicarbazonato nickel (II) **(2b)** and bis-3-benzyl-7,8-dimethoxycoumarin–thiosemicarbazonato cobalt (II) **(2c)**, against the BChE target are shown as −5.92 and −3.97 kcal/mol, respectively, in Table 3. In vitro analysis reveals the corresponding

Table 3. The binding energy (BE) analysis of compounds **2a**, **2b**, **2c**, Tacrine and Acarbose.

Enzyme	2a	2b	2c	Tacrine[a]	Acarbose[b]
	BE (kcal/mol)				
AChE	−102.34		−25.46	*−7.37*	
BChE		−5.92	−3.97	*−6.81*	
α-Gly		−39.41	−39.46		*−7.53*
α-Amy	−10.41		−9.49		*−5.37*

[a] Tacrine is as a positive control for AChE and BChE. [b] Acarbose is as a positive control for α-glucosidase and α-amylase.

© 2023 Wiley-VCH GmbH

23656549, 2023, 38, Downloaded from https://chemistry-europe.onlinelibrary.wiley.com/doi/10.1002/slct.202301786 by Marmara University, Wiley Online Library on [06/11/2023]. See the Terms and Conditions (https://onlinelibrary.wiley.com/terms-and-conditions) on Wiley Online Library for rules of use; OA articles are governed by the applicable Creative Commons License

numerical values of the compounds to be 115.84±13.68 and 129.64±10.74 in Table 2. To shed light on this at the atomic level, compound **2b** (cobalt metal complex) exhibits the best binding and interactions with the enzyme. As depicted in Figure 5, both in two and three dimensions, the orientation and interactions in the active site of the target enzyme are demonstrated. The compound **2b** forms hydrogen bonds with Pro285, Asp70, Ser287, Thr120, Gln67, and Trp82 residues of the target enzyme. Additionally, it engages in sulfur X-bond with Asp70, electrostatic interaction with His438, pi-cation interaction with Trp231, and hydrophobic interactions with Pro285, His438, Phe329, His438, Trp231, Val288, Pro84, Ile69, Leu286, and Ala328 residues of BChE. In other words, the non-bonding binding interactions contributing to the experimental activity of the compound **2b** and the orientation of the relevant compound in the active region of the target enzyme are illuminated.

On the other hand, the compound **2c** exhibits fewer types of interactions compared to the compound **2b**. The most significant reason for this difference is the optimal conformation of each compound in the active site of the present protein. The reference compound, tacrine, in the binding region of BChE, forms less binding tendency with the target than the two strong complexes, primarily due to its structural and orientational position, as shown in Figure 5. Meanwhile, the details of the interactions are provided at Table S1 in supplementary file.

Diabetes is characterized by chronic hyperglycemia and has become an important health problem all over the world. A persistently high level of glucose in the blood leads to cardiovascular diseases, neuropathy, retinopathy, nephropathy, and other dysfunctions. The hypoglycemic drugs used today manage to normalize the serum glucose level, but they cause gastrointestinal disturbances. Therefore, it is important to find effective therapeutic agents that inhibit α-glucosidase and α-amylase and have no side effects.[31] In these conditions, **2b** and **2c** complexes showing potential inhibitory activity against α-glucosidase protein were analyzed by docking simulation. As a result of docking calculations, their respective complex structures tend to bind better than the control compound of the related target, acarbose. Because newly synthesized Co and Ni metal complexes perform electrostatic, pi-sulfur, pi-lone pair, and hydrophobic interactions as well as H-bond interactions with α-Gly like the control compound. Especially as seen in Figure 6, **2c** has the best interaction with the enzyme with its binding energy value of −39.46 kcal/mol. The compound **2c** creates hydrogen bonds with Asn412, Arg312, Asp214, Asp68, and His 239 residues, electrostatic interactions with Glu304, Arg439, and Glu276, pi-sulfur interactions with Phe157, His279, Phe300, pi-lone pair interaction with Phe157 and hydrophobic interactions with Phe157, Val277, Ala278, Arg312, Lys155, Ile415, Tyr71, His111, Phe177, Phe311, Tyr313, Leu218, Arg439, and Pro309 amino acids of the target. On the other hand, bis-3-benzyl-7,8-dimethoxycoumarin–thiosemicarbazonato nickel (II) (**2b**) had the same type of interaction compared to bis-3-benzyl-7,8-dimethoxycoumarin–thiosemicarbazonato cobalt (II) (**2c**) with α-glucosidase, but due to a different orientation in the interaction, it resulted in a binding energy value of −39.41 kcal/mol. Additionally, as seen from the 2D interaction image, it

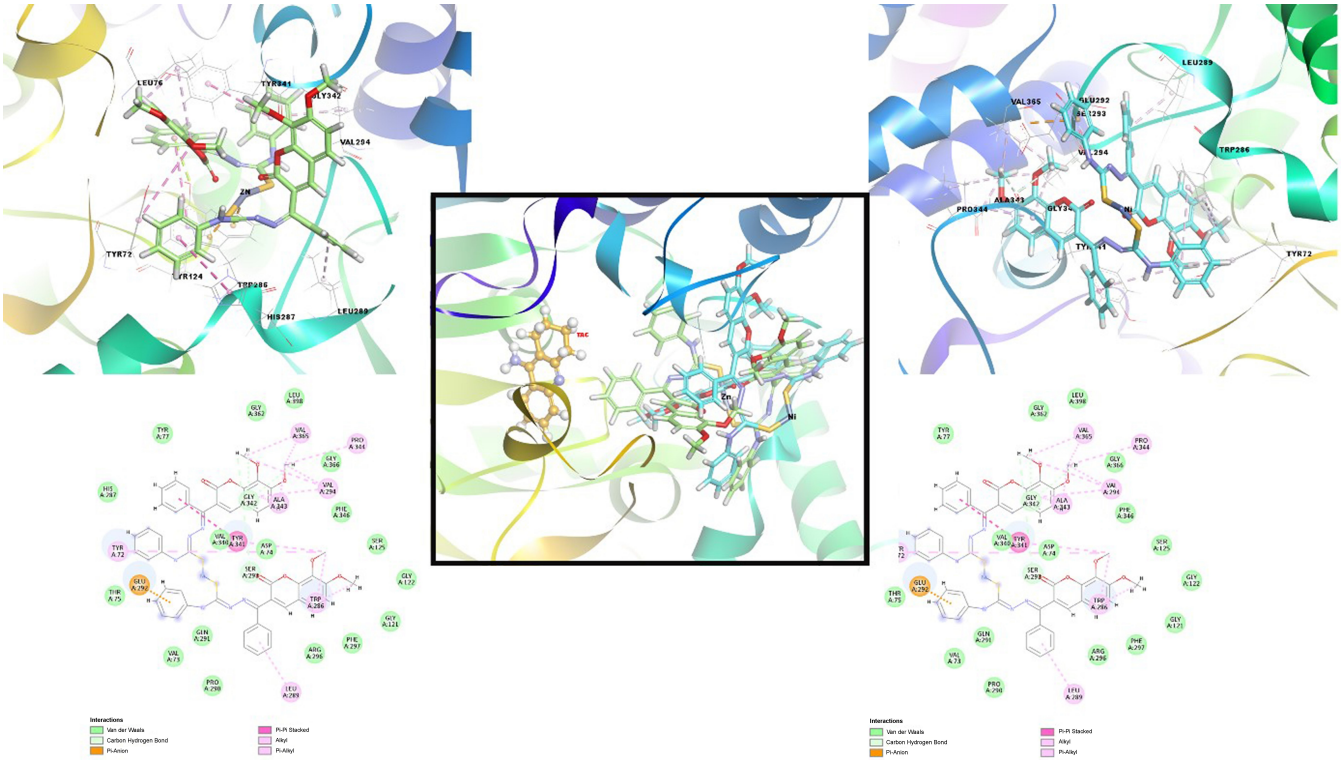

Figure 5. 3D binding modes and interactions of compounds **2a** and **2c** with AChE, superimposed state of the current compounds to Tacrine as reference compound of AChE.

© 2023 Wiley-VCH GmbH

23656549, 2023, 38, Downloaded from https://chemistry-europe.onlinelibrary.wiley.com/doi/10.1002/slct.202301786 by Marmara University, Wiley Online Library on [06/11/2023]. See the Terms and Conditions (https://onlinelibrary.wiley.com/terms-and-conditions) on Wiley Online Library for rules of use; OA articles are governed by the applicable Creative Commons License

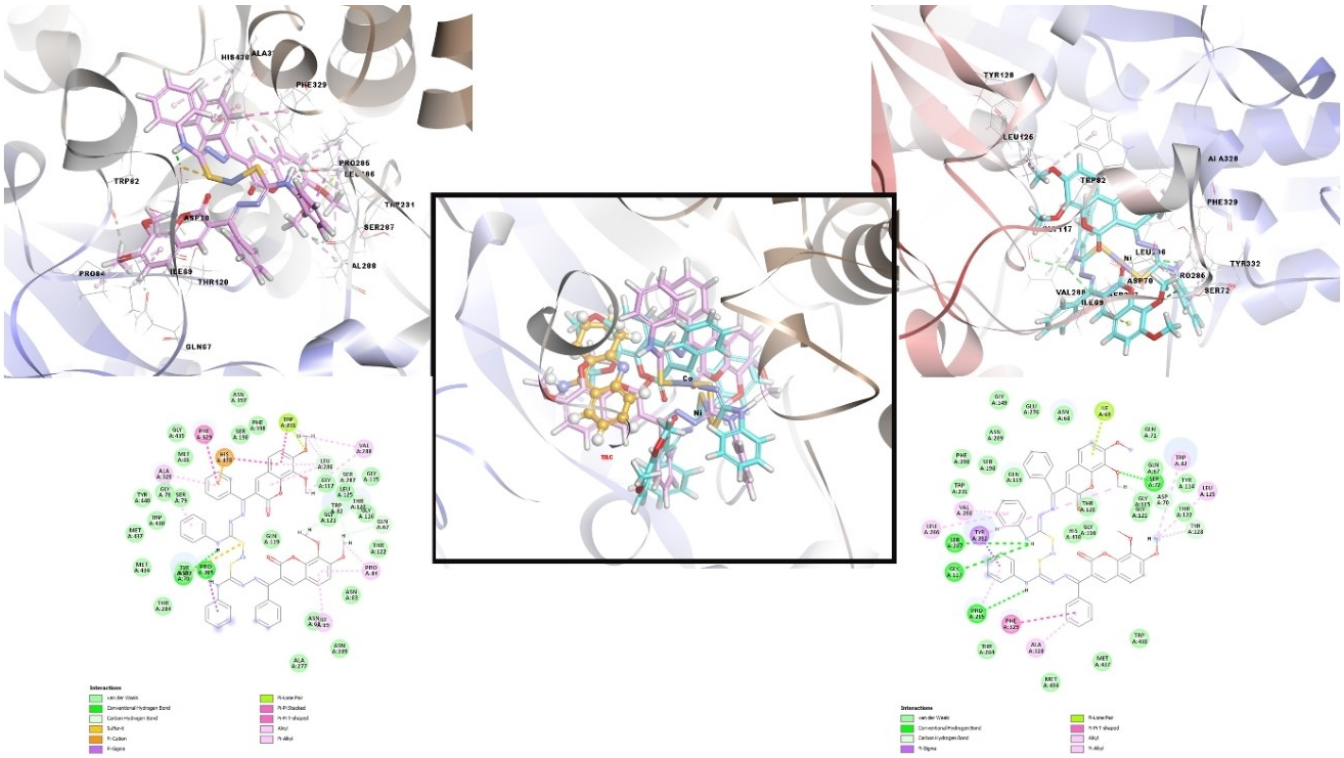

Figure 6. 3D binding modes and interactions of compounds **2b** and **2c** with BChE, superimposed state of the current compounds to Tacrine as reference compound of BChE.

forms undesired interactions with the target. This is indicated by highlighting the relevant residue in red. Consequently, compound **2b**, which is a nickel complex, has a lower target binding affinity than rhe compound (**2c**), which is a cobalt complex.

Finally, one of the new complexes containing α-amylase, compound **2a** [bis-3-benzyl-7,8-dimethoxycoumarin–thiosemicarbazonato zinc (II)], exhibited the best binding score with a binding energy of −10.41 kcal/mol. The control compound, acarbose, forms a highly hydrophilic interaction with the target, whereas in the interactions of Zn and Co metal complexes **2a** and **2c**, respectively, hydrophobic interactions prevail over hydrophilic interactions (Figure 7). Based on the results of in vitro analyses, computational studies emphasize the importance of hydrophilic interactions in the biological activity of the considered complex types with α-amylase. This is due to the larger polar surface area of the target's active site compared to the nonpolar surface area. This situation is visually presented in Figure 8 and detailed interaction information is provided in Supplementary Table S1.

Conclusions

This research reports that 3-benzoyl-7,8-methoxycoumarin, its new coumarin–thiosemicarbazone ligand, and zinc(II), nickel(II), and copper(II) metal complexes were synthesized and characterized. All synthesized metal complexes were tested on butyrylcholinesterase, acetylcholinesterase, α-amylase, and α-glucosidase enzymes. As a result, complex bis-3-benzyl-7,8-dimethoxycoumarin–thiosemicarbazonato zinc (II) **(2a)** can be considered a promising AChE inhibitor. Additionally, molecular docking studies have provided evidence for the dual inhibition of AChE and α-amylase species by compounds **2a** and **2c**. Conversely, compounds **2c** and **2b** have exhibited potential inhibitory activity against α-glucosidase. Both experimental and computational studies, the potential effectiveness of the interactions of metals, especially zinc metal, with organic compounds in dimeric form, with the targets under consideration cannot be ignored.

Experimental Section

Materials and Equipment

2-Hydroxy-3,4-dimethoxybenzaldehyde, ethyl benzoylacetate, phenylisothiocyanate hydrazine hydrate, $Co(OAc)_2 \cdot 4H_2O$, $Zn(OAc)_2 \cdot 2H_2O$, and $Ni(OAc)_2 \cdot 4H_2O$ were purchased from Sigma-Aldrich Chemicals. Synthesized new compounds were characterized by different methods such as FT-IR, UV-Vis, X-Ray, Maldi-TOF MS, ^{1}H-NMR, ^{13}C-NMR, and elemental analysis (For metal complexes; FT-IR, UV-Vis, MALDI-TOF-MS, elemental analysis). For FT-IR measurements ATR on the Perkin Elmer spectrum, two FT-IR Spectrometers were used. The C, H, N, and S microanalyses were studied on the LECO, CHNS-932 elemental analyzer. ^{1}H-NMR and ^{13}C-NMR chemical shifts were measured using DMSO-d_6 and recorded using a BRUKER DPX-400 spectrometer. The electronic spectra of the UV-Visible zone (250–800 nm) of all compounds were measured on a model Agilent UV-Vis spectrophotometer (1 cm quartz cell; in DMSO).

© 2023 Wiley-VCH GmbH

23656549, 2023, 38, Downloaded from https://chemistry-europe.onlinelibrary.wiley.com/doi/10.1002/slct.202301786 by Marmara University, Wiley Online Library on [06/11/2023]. See the Terms and Conditions (https://onlinelibrary.wiley.com/terms-and-conditions) on Wiley Online Library for rules of use; OA articles are governed by the applicable Creative Commons License

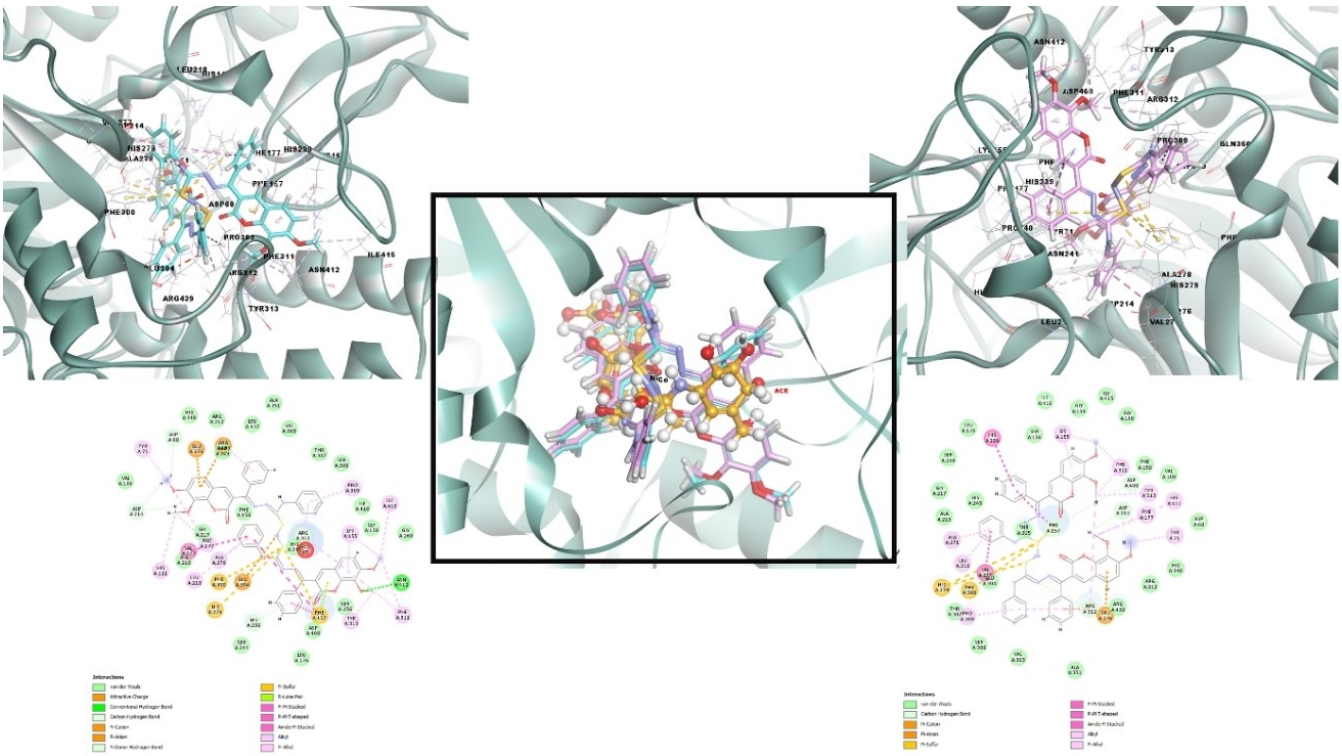

Figure 7. 3D binding modes and interactions of compounds **2 b** and **2 c** with α-Gly, superimposed state of the current compounds to Acarbose as reference compound of α-Gly.

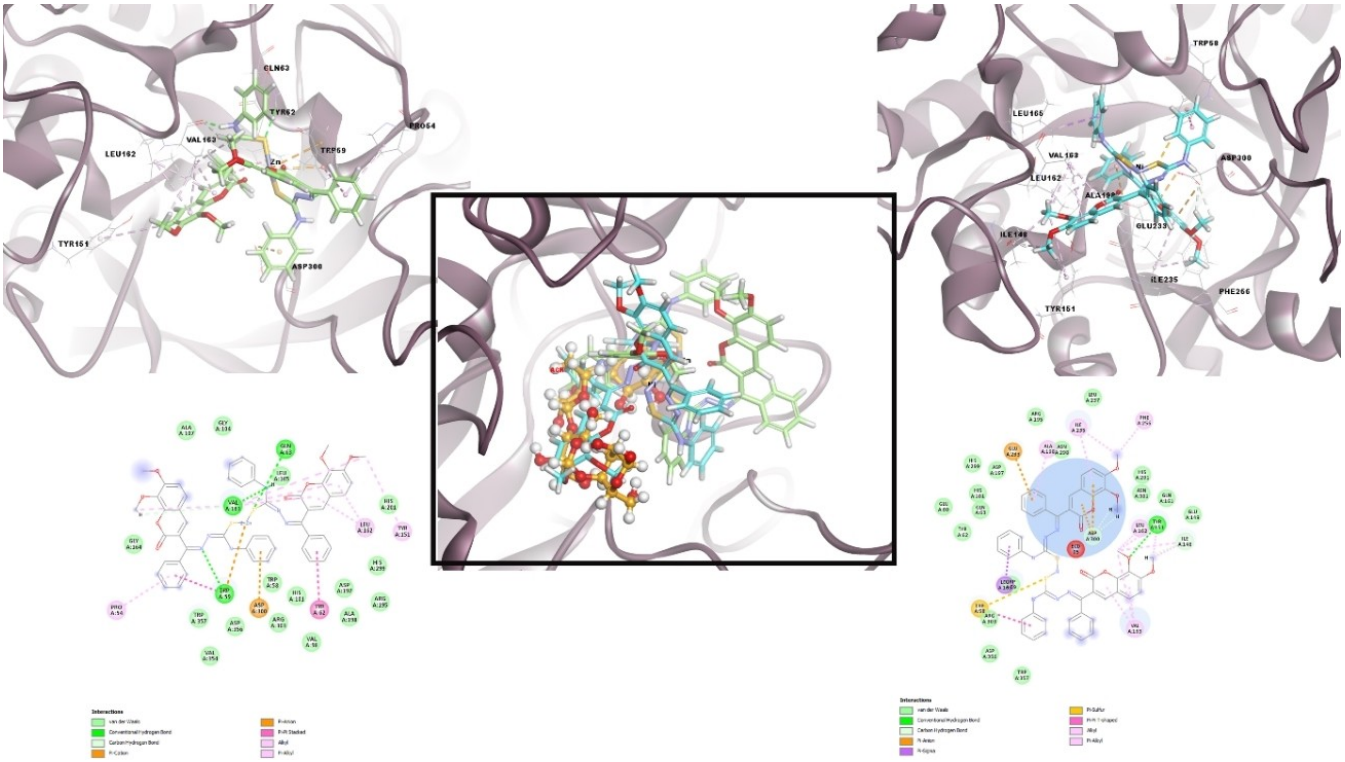

Figure 8. 3D binding modes and interactions of compounds **2 a** and **2 c** with α-Amy, superimposed state of the current compounds to acarbose (ACR) as reference compound of related target.

Synthesis

© 2023 Wiley-VCH GmbH

23656549, 2023, 38, Downloaded from https://chemistry-europe.onlinelibrary.wiley.com/doi/10.1002/slct.202301786 by Marmara University, Wiley Online Library on [06/11/2023]. See the Terms and Conditions (https://onlinelibrary.wiley.com/terms-and-conditions) on Wiley Online Library for rules of use; OA articles are governed by the applicable Creative Commons License

Synthesis of 3-benzoyl-7,8-dimethoxy coumarin (1) Knoevenagel reaction was used for the synthesis of the 3-benzoyl-7,8-dimethoxy-coumarin. 2-Hydroxy-3,4-dimethoxybenzaldehyde (2.00 g, 10.98 mmol) and ethyl benzoyl acetate (2.11 g, 10.98 mmol) dissolved in 20 mL ethanol. After adding 1.00 mL of piperidine, the reaction mixture was heated at 60 °C overnight. At the end of the period, the reaction mixture was poured into the ice water. The precipitate was filtered and washed with plenty of water and waited to dry. The resulting crude product was crystallized using an ethyl acetate/hexane solvent mixture. Yield: 72 %, light yellow-white crystal. Anal. Calc. for $C_{18}H_{14}O_5$: C, 69.67; H, 4.55; O, 25.78, found: C, 69.52; H, 4.30; O, 25.94 %. UV-Vis (DMSO, λ_{max}/nm) (logε): 350 (4.75). Selected FT-IR vibrations (cm^{-1}): 3063 (Aromatic C–H), 2943–2832 (Aliphatic C–H), 1711 and 1652 (C=O), 1600 (C=C), ^{1}H-NMR (DMSO-d_6, δ, ppm) 8.37 (s, 1H), 7.92 (d, 2H J = 7.80), 7.71–7.66 (m, 1H), 7.62 (d, 1H J = 8.77 Hz), 7.58–7.53 (m, 2H), 7.22 (d, 1H J = 8.66), 3.98 (s, 3H $-OCH_3$), 3.90 (s,3H $-OCH_3$). ^{13}C-NMR (DMSO-d_6, δ, ppm) 192. 32, 158.42, 157.33, 148.60, 146.91, 136.96, 135.54, 134.09, 129.92, 129.11, 126.02, 123.19, 113.33, 110.29, 61.34 and 57.07.

Synthesis of 4-phenyl thiosemicarbazide 4-Phenyl thiosemicarbazide was synthesized and purified according to the literature procedures.[32] A yield of 62 % was obtained.

Synthesis of (E)-2-((7,8-dimethoxy-2-oxo-2H-chromen-3-yl)(phenyl)methylene)-N-phenyl-hydrazine-1-carbothioamide (2) 3-Benzoyl-7,8-dimethoxycoumarin (**1**) (1.77 mmol, 0.50 g), and 4-phenyl thiosemicarbazide (2.12 mmol, 0.35 g) dissolved in 20 mL ethanol. After the addition of a drop of sulfuric acid as a catalyst, the reaction mixture was heated at 80 °C for one day. The reaction was terminated after the formation of a yellow precipitate. The mixture was then filtered and washed with water, then dried under a vacuum. The resulting product was crystallized using acetone. Yield: 81.25 %. The result of the crystallization color is yellow. Anal. Calc. For $C_{25}H_{21}N_3O_4S$: C, 65.35; H, 4.61; N, 9.14; S, 6.98, found: C, 64.70; H, 4.27; N, 9.44; S, 6.75 %. UV-Vis (DMSO, λ_{max}/nm) (logε): 328 (4.84). Selected FT-IR vibrations (cm^{-1}): 1717 (C=O), 1604 (C=N), 1366 (C=S), 3290 (N–H). ^{1}H-NMR (DMSO-d_6, δ, ppm) 11.29 (s, 1H), 10.26 (s, 1H), 8.08 (s, 1H), 7.92 (d, 2H, J = 8.14 Hz), 7.58 (d, 2H, J = 7.78 Hz), 7.52 (d, 1H, J = 8.5), 7.45–7.38 (m, 5H), 7.26 (t, 1H, J = 6.83 and J = 6.91 Hz), 7.20 (d, 1H, J = 8.81), 3.97 (s, 3H $-OCH_3$), 3.93 (s, 3H $-OCH_3$). ^{13}C-NMR (DMSO-d_6, δ, ppm) 177.63, 158.70, 156,29, 148.44, 145.63, 143,43, 139.61, 136.49, 135.61, 130.13, 128.87, 128.57, 127.89, 126.69, 124.66, 118.97, 114.43, 109.71, 61.34 and 57.04.

General procedure for the preparation of the metal complexes (2 a–2 c) A general method was used for the preparation of complexes using the reaction of metal salts and compound **2** in a molar ratio (M:L = 1:2). Compound **2** and one of the metal salts [Zn-$(OAc)_2 \cdot 2H_2O$ for **2 a**, $Ni(OAc)_2 \cdot 4H_2O$ for **2 b**, and $Co(OAc)_2 \cdot 4H_2O$ for **2 c**] were dissolved in 15 mL ethanol after the addition of one drop Et_3N. The reaction mixtures were refluxed for 4 hours and the nickel complex (**2 b**) was further stirred at room temperature for an additional 2 days. The reaction resulted in orange precipitate for zinc complex, brick red precipitate for nickel complex and brown precipitate for cobalt complex. After that, the precipitates were filtered and air-dried. These products were purified by washing with acetone and diethyl ether (Scheme 1).

(2 a) Orange solid. Yield: 92.45 %, $C_{50}H_{40}N_6O_8S_2Zn$. MALDI-TOF-MS: 982.30 $[M]^+$. Anal. Calc.: C, 61.13; H, 4.10; N, 8.55; S, 6.53 %, found: C, 61.64; H, 4.06; N, 8.70; S, 6.83 %. UV-Vis (DMSO, λ_{max}/nm): 277, 392. Main FT-IR vibrations (cm^{-1}): 1731 (C=O), 1590 (C=N), 1285 (C=S), 401 (M–O), 498 (M–N). The complex is soluble in DMF and DMSO.

(2 b) Brown-reddish solid. Yield: 55 %, $C_{50}H_{40}N_6NiO_8S_2$. MALDI-TOF-MS: 976.92 $[M+H]^+$. Anal. Calc.: C, 61.55; H, 4.13; N, 8.61; S, 6.57 %, found: C, 61.76; H, 4.20; N, 8.39; S, 6.43 %. UV-Vis (DMSO, λ_{max}/nm): 261, 338, 486. Main FT-IR vibrations (cm^{-1}): 1591 (C=N), 1289 (C=S), 400 (M–O), and 521 (M–N). The complex is soluble in DMF and DMSO.

(2 c) Brown solid. Yield: 60 % $C_{50}H_{40}CoN_6O_8S_2$ Mw: 975.96 MALDI-TOF-MS: 975.39 $[M]^+$. Anal. Calc.: C, 61.53; H, 4.13; N, 8.61; S, 6.57 %, found: C, 61.66; H, 4.10; N, 8.55; S, 6.33 %. UV-Vis (DMSO, λ_{max}/nm): 276, 366, 471. Main FT-IR vibrations (cm^{-1}): 1586 (C=N), 1290 (C=S), 407 (M–O), and 502 (M–N). The complex is soluble in DMF and DMSO.

Enzyme Studies

ChE inhibitory abilities of the new compounds against AChE and BChE were determined by Ellman's method, and this method was based on previous studies. Inhibitions of these enzymes were evaluated spectrophotometrically at a wavelength of 412 nm. α-Glycosidase inhibitory abilities of new compounds were determined according to the reported method by Tao *et al.* and this method was based on previous studies. The absorbance was spectrophotometrically measured at 405 nm.

Theoretical Calculations

Prior to docking, we evaluated the accuracy of the docking approach by re-docking of Tacrine and/or -Acarbose as standard ligands into each target model in this research Next, ligand(s) and related enzymes were prepared using software Gaussian 09 (G09)[33] and Discovery Studio (DS) 3.5.[34] The 2D chemical structures of the synthesized Zn, Co, and Ni metal complexes (**2 a**–**2 c**) were drawn by GaussView 5.0,[35] and then geometry and energy optimization were made at MO–G/PM6 basis set with SCIGRESS software.[36] Furthermore, their conformational analysis were performed using Discovery Studio (DS) 3.5. As target structures, AChE (PDB: 7XN1), BChE (PDB: 4BDS), α-amylase (α-Amy) (PDB: 1DHK) structures were taken from the protein database.[37] In our study, in vitro studies were conducted against α-glucosidase enzyme derived from Saccharomyces cerevisiae. In this context, due to the lack of a three-dimensional structure of the glucosidase enzyme, docking studies were performed using the model structure we previously constructed and the homology modeling method.[38] Hydrogen and missing heavy atoms were added to the protein structure, and atom types and partial charges were assigned. The positions of four target proteins were then optimized using the CHARMm force field and the Adapted Basis Newton-Raphson (ABNR) method available in DS 3.5 protocol[39] until the root mean square deviation (RMSD) reached below 0.05 kcal/mol Å^2. The binding site was defined using the "Define and Edit Binding Site" section in the DS software and information from the literature. The docking input grid files were prepared from the PDB complex structures using AutoDockTools 1.5.7, and docking was performed using AutoDock 4.2.[40] During preparation, an energy grid box of dimensions (126, 126, 126 Å) was set in the x, y, and z directions. These parameters were based on the size of each enzyme's binding region and the binding coordinates of the co-crystal ligand. The Lamarckian genetic algorithm was chosen for conformational search, and 200 independent docking runs were performed for each compound. AutoDock software assigned random torsional angles to each rotatable bond. The binding energy of each ligand pose was calculated, and protein-ligand interactions were analyzed using DS 3.5. Additionally, the obtained results were evaluated with reference to Tacrine (TAC) compound for the first two enzymes and Acarbose (ACR) compound for the last two enzymes.

© 2023 Wiley-VCH GmbH

23656549, 2023, 38, Downloaded from https://chemistry-europe.onlinelibrary.wiley.com/doi/10.1002/slct.202301786 by Marmara University, Wiley Online Library on [06/11/2023]. See the Terms and Conditions (https://onlinelibrary.wiley.com/terms-and-conditions) on Wiley Online Library for rules of use; OA articles are governed by the applicable Creative Commons License

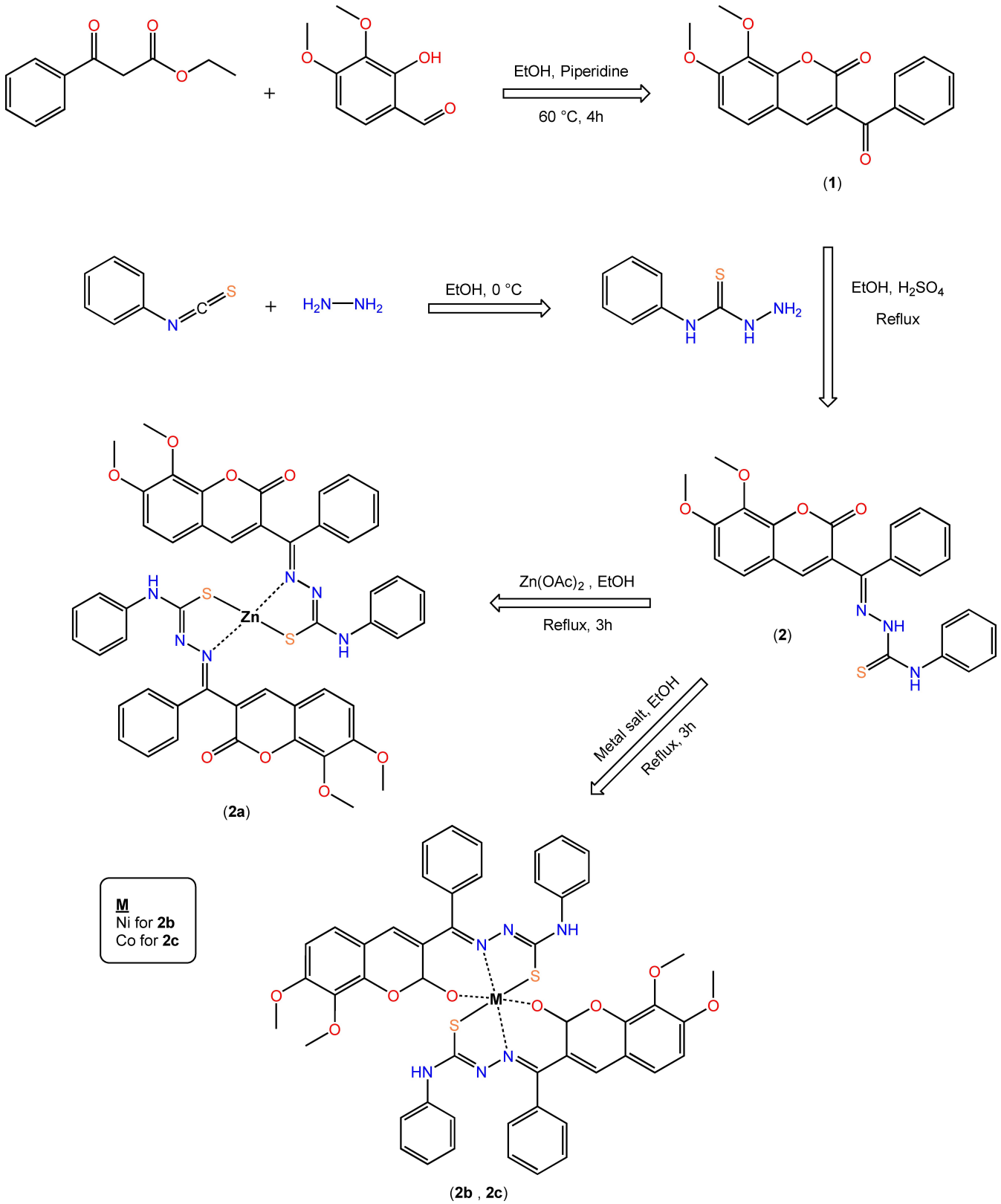

Scheme 1. The reaction scheme of 3-benzoyl-7,8-dimethoxycoumarin (**1**), 4-phenyl thiosemicarbazide, (E)-2-((7,8-dimethoxy-2-oxo-2*H*-chromen-3-yl)(phenyl)methylene)-*N*-phenylhydrazine-1-carbothioamide (**2**) and its Zn, Ni and Co metal complexes (**2a**, **2b**, and **2c**).

Single Crystal X-Ray Parameters

The Single-Crystal X-Ray Diffraction data of **1** and **2** were obtained with a Bruker APEX II QUAZAR three-circle diffractometer. Indexing

© 2023 Wiley-VCH GmbH

23656549, 2023, 38, Downloaded from https://chemistry-europe.onlinelibrary.wiley.com/doi/10.1002/slct.202301786 by Marmara University, Wiley Online Library on [06/11/2023]. See the Terms and Conditions (https://onlinelibrary.wiley.com/terms-and-conditions) on Wiley Online Library for rules of use; OA articles are governed by the applicable Creative Commons License

was performed using APEX2.[41] The structures of **1** and **2** were solved using SHELXT[42] and then refined by full-matrix least-squares refinements on F2 using SHELXL[43] in the Olex2 Software.[44] The positions of all H-atoms bonded to aromatic carbon atoms were geometrically optimized by HFIX 43 instructions in SHELXL and finally, Mercury 4.0 Software[45] was used for visualization of the CIF (Crystallographic Information Files) and calculation of bond lengths, torsion, and bond angles. Deposition Number(s) 2214759 (for **1**) and 2214757 (for **2**) contain(s) the supplementary crystallographic data for this paper. These data are provided free of charge by the joint Cambridge Crystallographic Data Centre and Fachinformationszentrum Karlsruhe Access Structures service.

Supporting Information

^{1}H-NMR, ^{13}C-NMR, MALDI-TOF-MS spectra and additional data of molecular docking and crystals are given in supporting information.

Acknowledgements

The authors thank Esin Akı Yalcin and the research group for the technical assistance. We are thankful to Türkiye Kimya Derneği. The numerical calculations reported in this paper were partially performed at TUBITAK ULAKBIM, High Performance and Grid Computing Center (TRUBA resources). This work was supported by the Research Foundation of Marmara University, Commission of Scientific Research Project (BAPKO) FYL-2022-10402.

Conflict of Interests

All authors declare that they have no conflicts of interest.

Data Availability Statement

The data that support the findings of this study are available in the supplementary material of this article.

Keywords: Acetylcholinesterase · Alpha-Amylase · Alpha-Glucosidase · Butyrylcholinesterase · Coumarin–Thiosemicarbazide

[1] a) R. Murray, *Nat. Prod. Rep.* **1989**, *6*, 591–624; b) A. Estévez-Braun, A. G. González, *Nat. Prod. Rep.* **1997**, *14*, 465–475.
[2] a) S. Nad, H. Pal, *J. Phys. Chem. A* **2001**, *105*, 1097–1106; b) A. Bouhaoui, M. Eddahmi, M. Dib, M. Khouili, A. Aires, M. Catto, L. Bouissane, *ChemistrySelect* **2021**, *6*, 5848–5870; c) H. Li, L. Cai, Z. Chen, *Adv. Chem Sen.* **2012**, *1*, 121–150.
[3] a) Y. Kong, Y.-J. Fu, Y.-G. Zu, F.-R. Chang, Y.-H. Chen, X.-L. Liu, J. Stelten, H.-M. Schiebel, *Food Chem.* **2010**, *121*, 1150–1155; b) M. Sanduja, J. Gupta, H. Singh, P. P. Pagare, A. Rana, *J. Saudi Chem. Soc.* **2020**, *24*, 251–266; c) B. M. Chougala, S. Samundeeswari, M. Holiyachi, N. S. Naik, L. A. Shastri, S. Dodamani, S. Jalalpure, S. R. Dixit, S. D. Joshi, V. A. Sunagar, *Eur. J. Med. Chem.* **2018**, *143*, 1744–1756.
[4] a) S. Emami, S. Dadashpour, *Eur. J. Med. Chem.* **2015**, *102*, 611–630; b) M. Kaur, S. Kohli, S. Sandhu, Y. Bansal, G. Bansal, *Anti-Cancer Agents Med. Chem.* **2015**, *15*, 1032–1048.
[5] a) S. Mishra, A. Pandey, S. Manvati, *Heliyon* **2020**, *6*, e03217; b) M. Z. Hassan, H. Osman, M. A. Ali, M. J. Ahsan, *Eur. J. Med. Chem.* **2016**, *123*, 236–255.
[6] a) L. Gao, F. Wang, Y. Chen, F. Li, B. Han, D. Liu, *Fitoterapia* **2021**, *154*, 104947; b) O. Danis, B. Yuce-Dursun, C. Gunduz, A. Ogan, G. Sener, M. Bulut, A. Yarat, *Arzneim.-Forsch.* **2010**, *60*, 617–620.
[7] a) T. S. Lobana, R. Sharma, G. Bawa, S. Khanna, *Coord. Chem. Rev.* **2009**, *253*, 977–1055; b) S. Konstantinović, B. Radovanović, A. Krklješ, *J. Therm. Anal. Calorim.* **2007**, *90*, 525–531.
[8] S. Eğlence-Bakır, O. Sacan, M. Şahin, R. Yanardag, B. Ülküseven, *J. Mol. Struct.* **2019**, *1194*, 35–41.
[9] A. Castiñeiras, N. Fernández-Hermida, I. García-Santos, L. Gómez-Rodríguez, *Dalton Trans.* **2012**, *41*, 13486–13495.
[10] S. Chandra, M. Tyagi, *Phosphorus, Sulfur, Silicon* **2009**, *184*, 778–789.
[11] N. V. Kulkarni, V. K. Revankar, B. Kirasur, M. H. Hugar, *Med. Chem. Res.* **2012**, *21*, 663–671.
[12] K. Bajaj, R. M. Buchanan, C. A. Grapperhaus, *J. Inorg. Biochem.* **2021**, *225*, 111620.
[13] D. Kovala-Demertzi, M. A. Demertzis, J. Miller, C. Papadopoulou, C. Dodorou, G. Filousis, *J. Inorg. Biochem.* **2001**, *86*, 555–563.
[14] M. Huseynova, V. Farzaliyev, A. Medjidov, M. Aliyeva, M. Özdemir, P. Taslimi, Y. Zorlu, B. Yalçın, O. Şahin, *J. Mol. Struct.* **2022**, *1248*, 131470.
[15] P. Heffeter, V. F. Pape, É. A. Enyedy, B. K. Keppler, G. Szakacs, C. R. Kowol, *Antioxid. Redox Signaling* **2019**, *30*, 1062–1082.
[16] M. Bingul, E. Şenkuytu, M. F. Saglam, M. Boga, H. Kandemir, I. F. Sengul, *Res. Chem. Intermed.* **2019**, *45*, 4487–4499.
[17] C. S. Rye, S. G. Withers, *Curr. Opin. Chem. Biol.* **2000**, *4*, 573–580.
[18] a) A. Chatonnet, O. Lockridge, *Biochem. J.* **1989**, *260*, 625; b) R. M. Lane, S. G. Potkin, A. Enz, *Int. J. Neuropsychopharmacol.* **2006**, *9*, 101–124; c) J. Massoulié, J. Sussman, S. Bon, I. Silman, *Prog. Brain Res.* **1993**, *98*, 139–146.
[19] a) P. K. Mukherjee, V. Kumar, M. Mal, P. J. Houghton, *Phytomedicine* **2007**, *14*, 289–300; b) N. Ranjan, M. Kumari, *Ann. Plant Sci.* **2017**, *6*, 1640–1644.
[20] D. Karcz, K. Starzak, E. Ciszkowicz, K. Lecka-Szlachta, D. Kamiński, B. Creaven, H. Jenkins, P. Radomski, A. Miłoś, L. Ślusarczyk, A. Matwijczuk, *Int. J. Mol. Sci.* **2022**, *23*, 6314.
[21] H. Çelik Onar, E. M. Özden, H. D. Taslak, İ. Gülçin, A. Ece, E. Erçağ, *Chem.-Biol. Interact.* **2023**, *383*, 110655.
[22] K. M. Amin, D. E. Abdel Rahman, H. Abdelrasheed Allam, H. H. El-Zoheiry, *Bioorg. Chem.* **2021**, *110*, 104792.
[23] S. Hamulakova, L. Janovec, M. Hrabinova, K. Spilovska, J. Korabecny, P. Kristian, K. Kuca, J. Imrich, *J. Med. Chem.* **2014**, *57*, 7073–7084.
[24] L. Dinparast, S. Hemmati, G. Zengin, A. A. Alizadeh, M. B. Bahadori, H. S. Kafil, S. Dastmalchi, *ChemistrySelect* **2019**, *4*, 9211–9215.
[25] a) D. Secci, S. Carradori, A. Bolasco, P. Chimenti, M. Yáñez, F. Ortuso, S. Alcaro, *Eur. J. Med. Chem.* **2011**, *46*, 4846–4852; b) A. Ameryckx, L. Pochet, G. Wang, E. Yildiz, B. E. Saadi, J. Wouters, F. Van Bambeke, R. Frédérick, *Eur. J. Med. Chem.* **2020**, *200*, 112444.
[26] a) C. T. G. Retnam, S. V. Rose, B. S. Kumari, *J. Mol. Struct.* **2023**, *1282*, 135162; b) M. Shebl, M. A. El-ghamry, S. M. E. Khalil, M. A. A. Kishk, *Spectrochim. Acta Part A* **2014**, *126*, 232–241; c) K. K. Abid, B. F. Abbas, *Res. Chem. Intermed.* **2012**, *39*, 3991–3999.
[27] a) R. H. Abu-Eittah, B. A. H. El-Tawil, *Can. J. Chem.* **1985**, *63*, 1173–1179; b) O. D. Kachkovski, O. I. Tolmachev, L. O. Kobryn, E. E. Bila, M. I. Ganushchak, *Dyes Pigm.* **2004**, *63*, 203–211; c) K. Pršir, E. Horak, M. Kralj, L. Uzelac, S. Liekens, I. M. Steinberg, S. Krištafor, *Molecules* **2022**, *27*, 637.
[28] H.-Y. Yin, J. Tang, J.-L. Zhang, *Chin. Chem. Lett.* **2018**, *29*, 267–270.
[29] a) F. Topkan, M. Özdemir, B. N. Özkan, K. Bozali, E. M. Güler, Y. Zorlu, M. Bulut, A. O. Görgülü, B. Yalçın, *Acta Crystallogr. Sect. D* **2022**, *78*; b) Q. Li, Y. Zhao, Z. Niu, E. Wang, *J. Fluoresc.* **2022**, *32*, 1443–1448; c) E. Budzisz, B. K. Keppler, G. Giester, M. Wozniczka, A. Kufelnicki, B. Nawrot, *Eur. J. Inorg. Chem.* **2004**, *2004*, 4412–4419; d) S. Aslkhademi, N. Noshiranzadeh, M. S. Sadjadi, K. Mehrani, N. Farhadyar, *Polyhedron* **2019**, *160*, 115–122.
[30] A. Hameed, M. Yaqub, M. Hussain, A. Hameed, M. Ashraf, H. Asghar, M. M. Naseer, K. Mahmood, M. Muddassar, M. N. Tahir, *RSC Adv.* **2016**, *6*, 63886–63894.
[31] S. Liu, Z. Ai, F. Qu, Y. Chen, D. Ni, *Food Chem.* **2017**, *234*, 168–173.
[32] V. Suni, M. P. Kurup, M. Nethaji, *Spectrochim. Acta Part A* **2006**, *63*, 174–181.

© 2023 Wiley-VCH GmbH

23656549, 2023, 38, Downloaded from https://chemistry-europe.onlinelibrary.wiley.com/doi/10.1002/slct.202301786 by Marmara University, Wiley Online Library on [06/11/2023]. See the Terms and Conditions (https://onlinelibrary.wiley.com/terms-and-conditions) on Wiley Online Library for rules of use; OA articles are governed by the applicable Creative Commons License

[33] M. Frisch, G. Trucks, H. Schlegel, G. Scuseria, M. Robb, J. Cheeseman, G. Scalmani, V. Barone, G. Petersson, H. Nakatsuji, X. Li, M. Caricato, A. Marenich, J. Bloino, B. Janesko, R. Gomperts, B. Mennucci, H. Hratchian, J. V. Ortiz, A. F. Izmaylov, J. L. Sonnenberg, D. Williams-Young, F. Ding, F. Lipparini, F. Egidi, J. Goings, B. Peng, A. Petrone, T. Henderson, D. Ranasinghe, V. Zakrzewski, J. Gao, N. Rega, G. Zheng, W. Liang, M. Hada, M. Ehara, K. Toyota, R. Fukuda, J. Hasegawa, M. Ishida, T. Nakajima, Y. Honda, O. Kitao, H. Nakai, T. Vreven, K. Throssell, J. Montgomery, J. Peralta, F. Ogliaro, M. Bearpark, J. Heyd, E. Brothers, K. Kudin, V. Staroverov, T. Keith, R. Kobayashi, J. Normand, K. Raghavachari, A. Rendell, J. Burant, S. Iyengar, J. Tomasi, M. Cossi, J. Millam, M. Klene, C. Adamo, R. Cammi, J. Ochterski, R. Martin, K. Morokuma, O. Farkas, J. Foresman, D. Fox, Wallingford, CT, **2016**.
[34] D. S. BIOVA, Dassault Systèmes San Diego, CA, USA, **2021**.
[35] R. Dennington, T. A. Keith, J. M. Millam, Semichem Inc.: Shawnee Mission, KS, USA, **2009**.
[36] N. Marchand, P. Lienard, H.-U. Siehl, H. Izato, *Fujitsu Sci. Tech. J.* **2014**, *50*, 46–51.
[37] Y. Rose, J. M. Duarte, R. Lowe, J. Segura, C. Bi, C. Bhikadiya, L. Chen, A. S. Rose, S. Bittrich, S. K. Burley, *J. Mol. Biol.* **2021**, *433*, 166704.
[38] a) K. P. Mugaranja, A. Kulal, *Heliyon* **2020**, *8,* e09360;b) D. Kısa, Z. Kaya, R. İmamoğlu, N. Genç, P. Taslimi, T. Taskin-Tok, *Arab. J. Chem.* **2022**, *15*, 103810.
[39] G. Wu, D. H. Robertson, C. L. Brooks, M. Vieth, *J. Comput. Chem.* **2003**, *24*, 1549–1562.
[40] O. Trott, A. J. Olson, *J. Comput. Chem.* **2010**, *31*, 455–461.
[41] Bruker, Bruker AXS Inc., Madison, WI, **2014**.
[42] G. Sheldrick, *Acta Crystallogr. Sect. A* **2015**, *71*, 3–8.
[43] G. M. Sheldrick, *Acta Crystallogr. Sect. C* **2015**, *71*, 3–8.
[44] O. V. Dolomanov, L. J. Bourhis, R. J. Gildea, J. A. Howard, H. Puschmann, *J. Appl. Crystallogr.* **2009**, *42*, 339–341.
[45] C. F. Macrae, I. Sovago, S. J. Cotrell, P. T. A. Galek, P. McCabe, E. Pidcock, M. Platings, S. P. Greg, J. S. Stevens, M. Towler, W. A. Peter, *J. Appl. Crystallogr.* **2020**, *1*, 226–235.

Manuscript received: July 6, 2023

© 2023 Wiley-VCH GmbH

23656549, 2023, 38, Downloaded from https://chemistry-europe.onlinelibrary.wiley.com/doi/10.1002/slct.202301786 by Marmara University, Wiley Online Library on [06/11/2023]. See the Terms and Conditions (https://onlinelibrary.wiley.com/terms-and-conditions) on Wiley Online Library for rules of use; OA articles are governed by the applicable Creative Commons License